Journal of Manufacturing Processes 75 (2022) 826–832

Contents lists available at ScienceDirect

Journal of Manufacturing Processes

journal homepage: www.elsevier.com/locate/manpro

A study on the sparking distance in the electrochemical discharging process

Yu-Jen Chen, Murali Sundaram *

Department of Mechanical and Materials Engineering, University of Cincinnati, Cincinnati, OH, USA

ARTICLE INFO

Keywords:
Electrochemical discharge machining
Gas film formation
Electrostatic force
Maximum sparking distance
Gas film collapsing

ABSTRACT

The electrostatic force affects the gas film formation and collapsing in the electrochemical discharge process. Experimental observation of the process using a side insulated tool shows that the gas bubble will collapse or depart from the tooltip at the removal of electrostatic force. This study investigates the relationship between the electrostatic force and the sparking distance. A unique experimental method is developed in this study to establish the distance of sparking. Within this distance the electrostatic force can attract the electrolyte to the tool and result in a spark. A mathematical model is developed to predict the sparking distance under the influence of electrostatic force. Experimental verification of the model revealed that the sparking distance could be reduced by decreasing the tool size and lowering the applied voltage. The model was able to predict the trend of the average sparking distance with less than 5% variation. Electrolyte concentration has a minor effect on the sparking distance but affects the voltage range for sparking.

1. Introduction

Electrical machining processes are increasingly gaining acceptance as material removal process in the manufacturing industry [1,2]. Particularly, electrochemical machining (ECM) and electrical discharge machining (EDM) are preferred to machine hardened conductive materials [3]. Electrochemical discharge machining (ECDM) is an emerging nontraditional electrical machining method that could machine conductive and non-conductive materials by electrical induced thermal and/or chemical machining [4–6]. ECDM involves electrochemical discharging (ECD) process, in which an anode and a cathode are immersed in an electrolyte with the workpiece placed near the tool (usually cathode). As the electrolysis occurs with the applied voltage greater than the critical voltage, gas bubbles (usually hydrogen) will be generated and coalesce into a gas film and gradually isolate the cathode from the electrolyte bath. Thermal removal of material happens when this gas film collapses, and a spark appears. In the ECD process, the sparking is highly related to the gas film conditions, and the sparking distance varies with the gas film thickness, which in turn is affected by the experimental conditions [7]. Thus, the gas film condition significantly influences the sparking distance and the machining accuracy.

Several studies that have been conducted to understand the effect of the gas film thickness in the ECD process performance revealed that the gas film thickness in ECD varied widely and affected the spark energy [6,8]. For example, the spark energy would increase with the increase in the gas film thickness [9,10]. The gas film thickness can be controlled by the electrode location and electrolyte condition [9]. Different mathematical models have been made to explain the gas film formation process and predict the gas film thickness [10,11]. A gas film model was presented for side insulated tools [10]. Another demonstrated the sparking process at the gas film below and above the critical voltage [10,11]. One model applied the departure size of gas bubbles to predict the formed average gas film thickness [12]. Another study used multiphase finite element simulation to understand the role of gas film in material removal [13]. It has been proposed that the sparking is caused by the small spacing between the adjacent gas bubbles; that is, as the bubbles are extremely crowded, the sparks would jump between the gaps and form the sparks [14]. The role of the high resistance [15] and the critical voltage [16] in the gas film formation and sparking process have also been studied.

However, none of these earlier works have correlated the sparking process with the gas film collapsing in the ECD process. The gas film collapsing process is related to the sparking or the gas bubble departure when the buoyance force overcomes the surface tension xn. These two forces are reported to be the two major forces affecting the departing process, while the inertia force on the gas bubble is assumed to be negligible [12]. It has been shown that the gas film formation process can be controlled by the electrostatic force [17]. In the present study, it is hypothesized that the electrostatic force plays a critical role in the gas film formation and collapsing in ECD. An experimental observation shows evidence of the hypothesis where the timing of gas film collapsing

* Corresponding author.
E-mail address: murali.sundaram@uc.edu (M. Sundaram).

https://doi.org/10.1016/j.jmapro.2022.01.048
Received 30 June 2021; Received in revised form 17 January 2022; Accepted 22 January 2022
Available online 1 February 2022

Nomenclature

D	initial distance
$\vec{E}$	electric field
R	radius of curvature for the electrolyte above surface level
V	applied voltage
$\vec{a}$	acceleration
d	tool diameter
f	fringing effect
$\vec{g}$	gravity constant
y	height of the electrolyte above surface level
m	mass of the electrolyte above surface level
q	charge on electrolyte surface
u	farthest horizontal distance of the electrolyte above surface level
γ	surface tension coefficient
ε	dielectric permeability
θ	angle at the projected edge of tool
ρ	electrolyte density
∅	angle of the surface tension
D_{max}	maximum sparking distance
$\vec{F_g}$	gravity force
$\vec{F_e}$	electrostatic force
$\vec{F_s}$	surface tension force
h_e	height of the electrolyte at the projected edge of tool

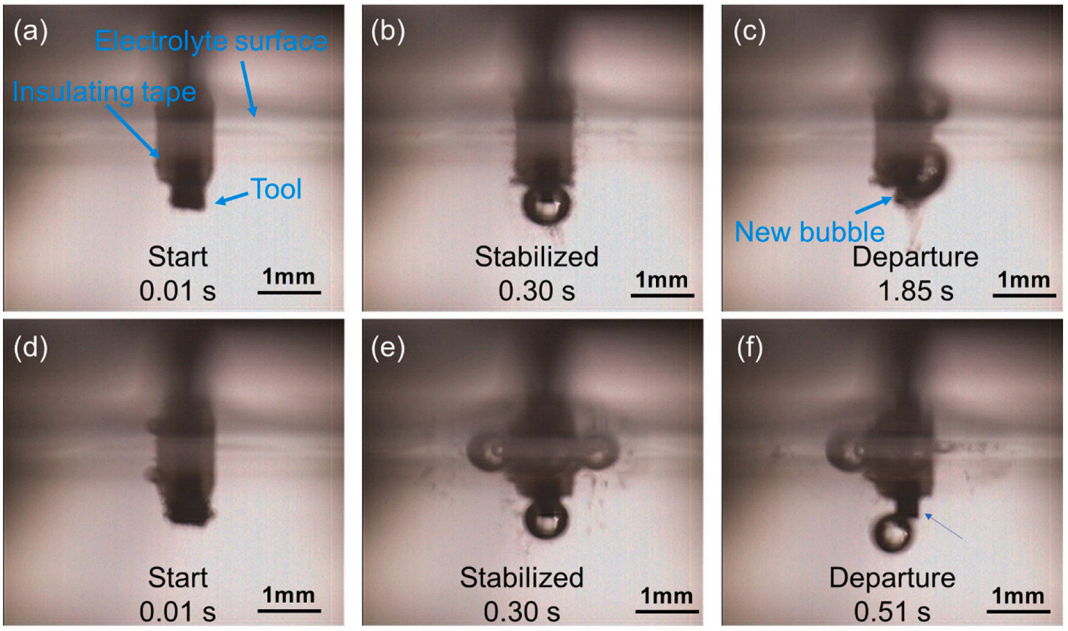

Fig. 1. Gas bubble formation and departure from a side insulated tool with (a)–(c) DC, (d)–(f) 1 Hz, 50% duty cycle pulse current.

process can be controlled by turning off the electrostatic force to force. A physics based theoretical model is made in this study to predict the gas film thickness under the influence of electrostatic force. Furthermore, a unique experimental method is used to validate the model.

2. Motivation

Two phenomena related to gas bubble departure and sparking as described below were observed in the preliminary ECD study, in which a 1 mm side insulated tool with tip immersed in NaOH electrolyte was used as the cathode as shown in Fig. 1. Images (a)–(c) and (d)–(f) are the observations made on gas bubble formation and departure from a side insulated tool with DC and pulsed current respectively.

(i) Gas bubble departure: A direct current (DC) and a pulse current with a 50% duty cycle at 1 Hz were applied to understand the role of the electrostatic force on the gas film formation and collapse. When DC was applied, a gas bubble formed at the tool tip, grew with time and departed in around 1.8–1.9 s when the buoyancy force overcame the attraction by surface tension and electrostatic force. However, in the case of pulse current, the bubble departure was found to be well synchronized with the end of pulse-on times (i.e. at 0.5, 1.5, 2.5 s and so on). The bubble will depart right when the pulse is off. When the current is switched off (pulse off), the bubble would immediately lose the electrostatic forces that held the bubble in place and start to depart as buoyance force is greater than surface tension. This provides an opportunity to break the insulation in much shorter time (0.5 s) as compared to DC. This shows that that the electrostatic force plays an important role in the gas bubble departure process.

(ii) Occurrence of sparks: The ECD process and the gas film collapsing/departure are generally found to occur simultaneously. The sparking occurred only once in the initial phase of bubble growth ($t < 0.3$ s) and ceased. No further sparking was observed till the gas bubble grew and departed (i.e., from 0.3 s to 1.5 s). Subsequently, the next spark occurred in the initial phase of the next bubble formation. In the case of DC, this waiting time is even longer (~2 s) as the electrostatic force holds the bubble for a longer time until the bubble grows sufficiently bigger for the buoyancy force to overcome the attraction forces. Here again, the sparking resumed only in the initial phase of the next bubble formation when the bubble size is small. This reveals the existence of optimal gas film thickness for the sparking to occur. When the gas film thickness exceeds this value, sparking pauses.

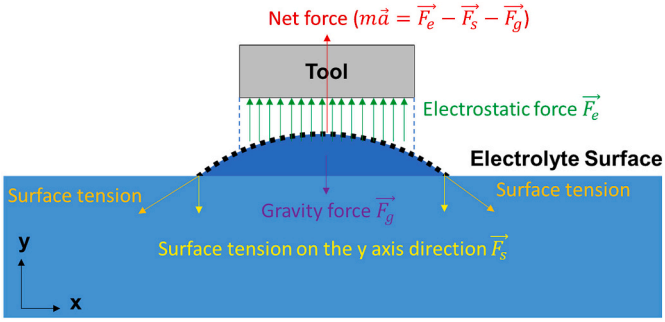

Fig. 2. A sketch of the force balance.

Thus, to increase the sparking frequency and productivity, it is hypothesized that the optimal gas film thickness can be achieved by controlling the electrostatic force. A physics-based model is created to understand the role of electrostatic force in the gas film formation process.

3. Theoretical model

In the proposed model, the sparking distance is predicted based on the electrostatic force, gravity, and surface tension involved in the force balance in ECD gas film.

The force balance in the gas film on the gravity direction (y-axis) can be described as

$$\vec{F_e} - \vec{F_s} - \vec{F_g} = \mathrm{m}\vec{a} \tag{1}$$

where $\vec{F_e}$ is the electrostatic force, $\vec{F_s}$ the surface tension on the y axis direction, and $\vec{F_g}$ the gravity force. $\vec{F_s}$ and $\vec{F_g}$ counters $\vec{F_e}$. $\mathrm{m}\vec{a}$ is the net force where m the mass of the pulled-up electrolyte by the electrostatic force and $\vec{a}$ the acceleration. A sketch of the force balance is shown in Fig. 2.

Following simplification assumptions are made in the development of the model:

- The surface tension remains constant.
- The electrostatic force only affects the electrolyte beneath the tool, and therefore, a rapid electrolyte level variation (level drop) occurs at the edge of the tool.
- Under the influence of electrostatic force, the surface of the electrolyte beneath the tool forms a curve with a radius of R which is applied in the surface tension calculation.
- The electrostatic force is calculated as a parallel plate capacitor (i.e., the tool and electrolyte surface) due to the small angle found in the raised electrolyte. The charges evenly distribute across the tool and electrolyte surface.
- The fringing effect f is applied [18]. Fringing or edge effect is the bending of the electric flux lines noticed near the edge of the parallel plate capacitors.
- The process of the tool approaching the electrolyte surface is assumed to be slow enough for the force to be static.
- Temperature change in the process is neglected.
- Substrate (i.e. workpiece) is not considered in the model.

By including the fringing effect of the electrostatic force, and using the first principles, Eq. (1) can be rewritten as:

$$\left(\frac{\mathrm{q}\vec{E}}{2}\right) - \vec{F_s} - \mathrm{m}\vec{g} = \mathrm{m}\vec{a} \tag{2}$$

where $\frac{\mathrm{q}\vec{E}}{2}$ is the electrostatic force $\vec{F_e}$ for a single plate from Lorentz

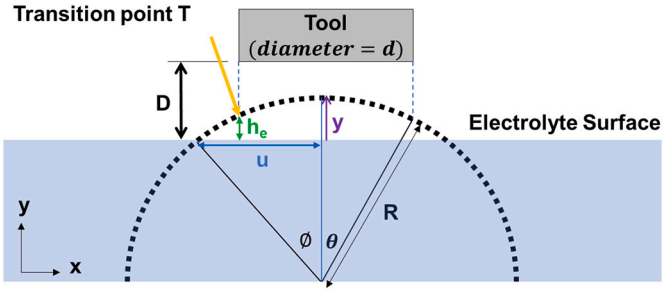

Fig. 3. An illustration of the geometry for the surface electrolyte model.

Force Law with $\mathrm{q} = \frac{\varepsilon \mathrm{A} V}{D}$ and $\left|\vec{E}\right| = \frac{V}{D}$. ε is the dielectric permeability of air, A the surface area of the tool, V the applied voltage, and D the initial gap between the tool and electrolyte. The surface tension $\vec{F_s}$ is the projection on the axis with $\left\|\vec{F_s}\right\| = \gamma L sin\varnothing$ and L equivalent to $2\pi u$, with γ is the surface tension coefficient, u the farthest distance of the pulled up electrolyte, and ∅ the angle of the surface tension. Finally, $\vec{F_g}$ is the gravity force on a spherical cap with $\mathrm{m} = \rho v$ where v is the volume of the electrolyte above the surface level and ρ the density of electrolyte. Fig. 3 shows an illustration of the tool and the electrolyte geometry under the influence of electrostatic force.

Eq. (2) can be expanded as:

$$\frac{1}{2}\varepsilon\pi f\left(\frac{\mathrm{d}}{2}\right)^2\left(\frac{V}{D}\right)^2 - 2\pi u\gamma \sin\varnothing - \frac{\pi\rho \mathrm{g} y^2}{3}(3R - y) = \mathrm{m}a \tag{3}$$

where f is the fringing effect [18]. Fringing effect is noticed at the edge of the tool, where the electrolyte is attracted by the extending electric flux outside of tool area. The fringing effect is $1 + \frac{2.55(D-y)}{\mathrm{d}}$ which is more noticeable as the gap between electrolyte and tool is larger or when the tool diameter is smaller. d is the tool diameter, y the height the electrolyte pulled-up, and R the radius of curvature for the pulled-up electrolyte surface. The surface tension γ of the electrolyte coefficient is taken as 7.5×10^{-2} N/m [19]; the density of electrolyte ρ is 1.05 kg/L [20]; the dielectric permeability of air ε is 8.85×10^{-12} F/m [21]; the gravity is 9.81 m/s^2.

Following the assumption, the electrostatic force will only affect the electrolyte right under the tool (i.e., the projected area under the tool), there should be a sudden electrolyte level drop at the projected edge of the tool. Therefore, the gravity force can be assumed to act on a cylindrical volume instead of a spherical cap and Eq. (3) can be simplified as

$$\frac{1}{2}\varepsilon\pi f\left(\frac{\mathrm{d}}{2}\right)^2\left(\frac{V}{D}\right)^2 - 2\pi u\gamma \sin\varnothing - \frac{\pi\rho \mathrm{g} \mathrm{d}^2 y}{4} = \mathrm{m}a \tag{4}$$

where $sin\varnothing = \sqrt{\frac{2y}{R} - \left(\frac{y}{R}\right)^2}$ and the radius of curvature of the electrolyte above surface level (R) is

$$R = \frac{\mathrm{d}}{2sin\theta} \tag{5}$$

To find R, a force balance is calculated at the transition point (T) where the electrostatic force has a lesser effect on the electrolyte outside of this point. The height of the electrolyte is h_e at this location. This model takes the projected edge of the tool on the electrolyte surface as the transition point. That is, at this transition point:

$$\sum \overrightarrow{F_{T,left}} = \sum \overrightarrow{F_{T,Right}} \tag{6}$$

The continuity of this point is not affected by the electrostatic force due to the assumption that the electrostatic force only affects the electrolyte beneath the tool. Thus, Eq. (6) can be written as:

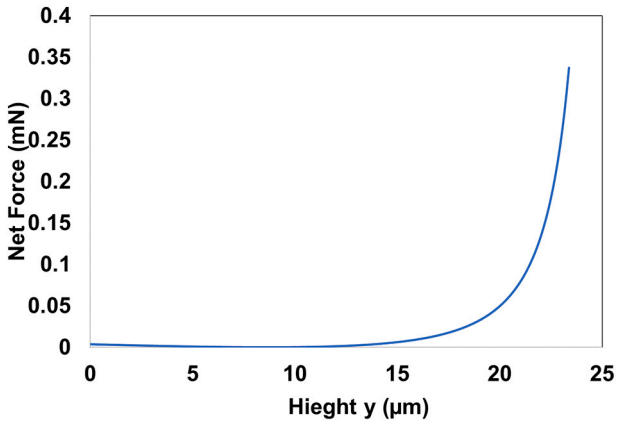

Fig. 4. The force calculated at an increasing height of electrolyte for a 26 μm initial gap with a 500 μm tool diameter and 50 V.

$$\overrightarrow{F_{s,T}} + \overrightarrow{F_{g,T}} \text{ (left)} = -\overrightarrow{F_{s,T}} + \overrightarrow{F_{g,T}} + \overrightarrow{F_{e,T}} \text{ (right)} \tag{7}$$

Thus, Eq. (7) in the presence and absence of electrostatic force can be written as given in Eq. (8).

$$2\overrightarrow{F_{s,T}} = \overrightarrow{F_{e,T}} \tag{8}$$

where $\left\|\overrightarrow{F_{s,T}}\right\| = 2\pi\gamma \mathrm{d}\sin\theta$ and $\left\|\overrightarrow{F_{e,T}}\right\| = \frac{1}{2}\varepsilon\pi f\left(\frac{\mathrm{d}}{2}\right)^2\left(\frac{V}{D-h_e}\right)^2$, $\mathrm{h_e}$ is the height of the electrolyte at this point. θ is the angle at this point and is found to be small (less than 3°) before reaching close to the tool where the electrostatic force dominates? Therefore, for the latter force calculation, h_e can be taken as y in the model. From Eq. (8) $\sin\theta$ can be expressed as

$$sin\theta = \frac{\varepsilon f \mathrm{d}}{16\gamma}\left(\frac{V}{D-y}\right)^2 \tag{9}$$

Thus, Eq. (5) can be rewritten as:

$$R = \frac{8\gamma}{\varepsilon f}\left(\frac{D-y}{V}\right)^2 \tag{10}$$

Finally, these values can be applied back to the force equilibrium function to find the sparking distance D. By substituting the expression for R into the surface tension on the y axis direction $\overrightarrow{F_s}$.

$$\left\|\overrightarrow{F_s}\right\| = 2\pi\gamma usin\varnothing = 2\pi\gamma\sqrt{R^2-(R-y)^2}\sqrt{\frac{2y}{R}-\left(\frac{y}{R}\right)^2} = 4\pi\gamma y - \frac{2\pi\gamma y^2}{R}$$
$$= 4\pi\gamma y - \frac{\varepsilon f\pi}{4}\left(\frac{yV}{D-y}\right)^2 \tag{11}$$

By substituting the expression for surface tension $\overrightarrow{\mathrm{F_s}}$ from Eq. (11) into Eq. (4) while taking the net force ma as a function we get:

$$\mathrm{f}(d,V,D,y) = \mathrm{ma} = \mathrm{k_1}f\left(\frac{\mathrm{d}}{2}\right)^2\left(\frac{V}{D-y}\right)^2 - \mathrm{k_2 y} - \mathrm{k_3}f\left(\frac{yV}{D-y}\right)^2 - \mathrm{k_4}\left(\frac{\mathrm{d}}{2}\right)^2 \tag{12}$$

where constants $\mathrm{k_1}$, $\mathrm{k_2}$, $\mathrm{k_3}$, and $\mathrm{k_4}$ are $\frac{1}{2}\varepsilon\pi$, $4\pi\gamma$, $\frac{\varepsilon\pi}{4}$, $\pi\rho g$ respectively. For a given input tool diameter d and voltage V, f(d,V,D,y) will become a function of D and y as shown in Eq. (13).

$$\mathrm{f}(D,\mathrm{y}) = \mathrm{m}a = \mathrm{c_1}\left(\frac{1}{D-y}\right)^2 - \mathrm{c_2}y - \mathrm{c_3}\left(\frac{y}{D-y}\right)^2 - \mathrm{c_4} \tag{13}$$

where constants $\mathrm{c_1}$, $\mathrm{c_2}$, $\mathrm{c_3}$, $\mathrm{c_4}$ are $\mathrm{k_1 f}\left(\frac{\mathrm{d}}{2}\right)^2\mathrm{V}^2$, $\mathrm{k_2}$, $\mathrm{k_3 f V}^2$, $\mathrm{k_4}\left(\frac{\mathrm{d}}{2}\right)^2$

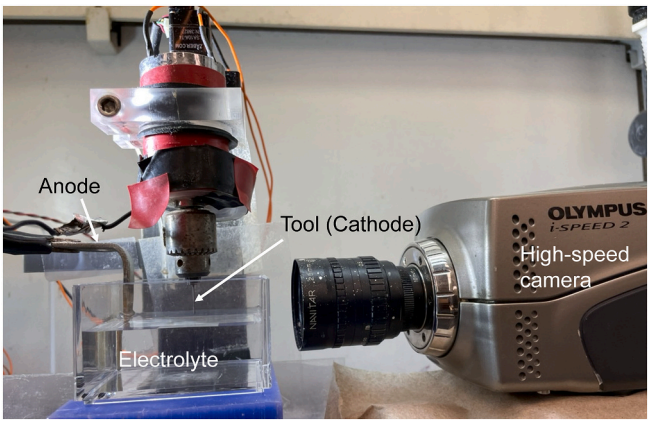

Fig. 5. The in-house built experimental setup.

Table 1
Parameters for the ECD machining.

Parameters	Values
Cathode	300–1000 μm cylinder WC
Applied voltage	30–60 V DC
Electrolyte	NaOH
Electrolyte concentration	0.5 M, 1 M, 5 M

respectively. Therefore, D can be written as Eq. (14).

$$D = y + \sqrt{\frac{\mathrm{c_1} - \mathrm{c_3}y^2}{\mathrm{m}a + \mathrm{c_2}y + \mathrm{c_4}}} \tag{14}$$

The acceleration should always be positive for the electrolyte to be continuously pulled upwards. That is, the net force is assumed to be always above 0 for any D and y value. Therefore, scanning though $D \in \mathrm{Q}$, D_{max} can be found at f(D, y) ∩ 0 while y is a range between 0 to D_{max}. An example of a D_{max} found at 50 V and 500 μm tool diameter is shown in Fig. 4.

4. Experimental method

The ECD experimental setup used for this study is shown in Fig. 5. A high-speed camera (Olympus I-speed) is used to characterize the gas film at 100 fps. The camera is adjusted to focus on the tool. A DC power supply with 0–120 V is applied. A precise stepper motor with 1.5 μm/step resolution controls the tool spindle. The experiments were performed using the list of parameters in Table 1.

The sparking distance was tested by controlling voltage. The tool is first positioned approximately 150 μm above the electrolyte surface. Then the tool is slowly (1.5 μm/s) moved down towards the electrolyte surface. When continuous sparking occurs, the power supply is turned off, and a timer is set to measure the time for the tool reaching the electrolyte surface. The maximum sparking distance is then calculated by multiplying the feed rate with the measured time. An image of the setup and the sparking process can be seen in Fig. 6(a) and (b), respectively. Different voltages, tool size, and electrolyte concentration are tested in this experiment.

5. Results and discussion

5.1. The effect of applied voltage on the sparking distance

The effect of voltage on the sparking distance is tested with a 500 μm tool in 1 M NaOH electrolyte. The voltage is decreased from 60 V to 40 V to find the sparking distance. Each experiment is repeated ten times in this study, and the average maximum sparking distance is recorded. The

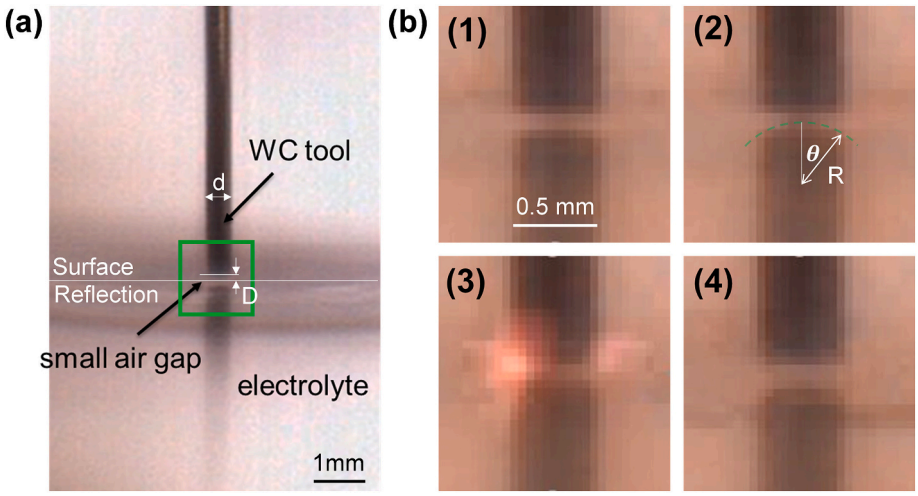

Fig. 6. (a) Image of the setup above the electrolyte surface. (b) The sequence of events in the sparking process was observed at the green boxed area in (a) after applying 60 V; 1 initial state; 2 electrolytes pulled upwards; 3 sparking; 4 electrolytes returning to initial state (new gas film formed). (For interpretation of the references to color in this figure legend, the reader is referred to the web version of this article.)

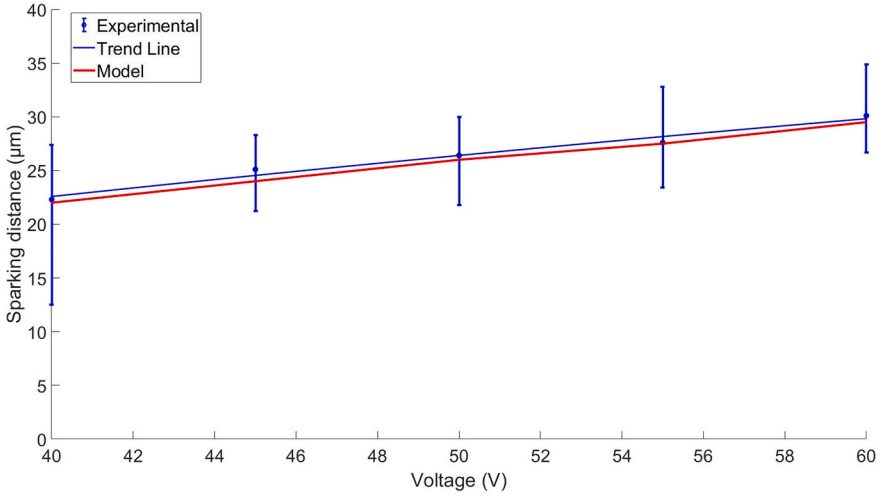

Fig. 7. Experimental data (bar) and model prediction (line) of the maximum sparking distance at different voltages.

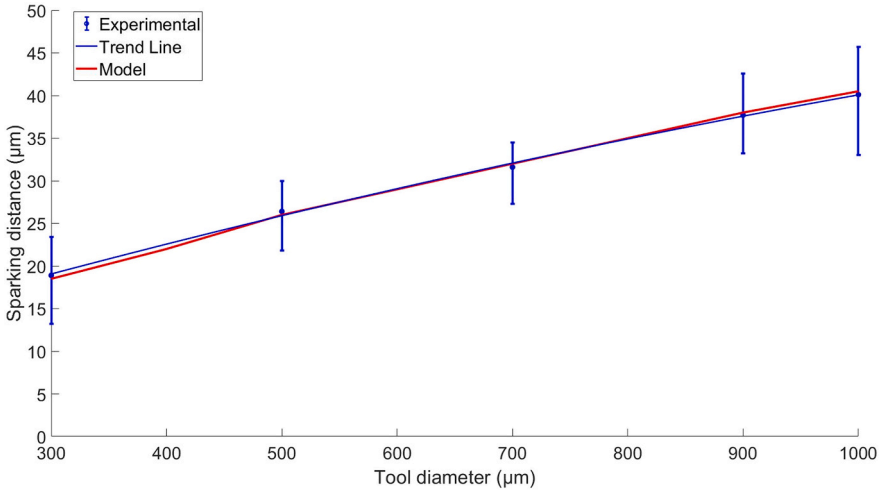

Fig. 8. Comparison of experimental data (bar) and model prediction (line) for the maximum sparking distance at different tool diameters.

Table 2
Maximum sparking distance (μm) on different experimental parameters with a 500 μm tool diameter.

Voltage (V)	NaOH 0.5 M	NaOH 1 M	NaOH 5 M
60	46	43	40
50		37	32
40		31	20
30			13

experimental results are verified with the model predictions, as shown in Fig. 7.

From Fig. 7, it can be seen that the model is capable of predicting the trend of the maximum sparking distance. The variation in between the prediction and the average sparking distance is less than 5%. The maximum sparking distance is proportional to the applied voltage, that is, the electrostatic force. An increasing force will be attaching the electrolyte surface from further beyond the surface of the electrolyte. In the experiment, sparking was not found below the critical voltage (35 V) for a 1 M NaOH. Therefore, voltages less than 35 V were not tested in this study. At 40 V (i.e. close to the critical voltage), the dispersion of sparking distance was found to be greater than other voltages tested. A possible reason is that instead of a spark, electrolysis occurs when the electrolyte approaches the tool, which delays the first sparking. However, the average is still found to be close to the model prediction. Overall, it was found that the maximum sparking distance would increase with the increase in the applied voltage as predicted by the model. The dispersion in the experimental data can be attributed to the turbulence of the electrolyte. The model shows that the maximum distance of sparking would be lesser at lower voltage as the electrostatic force is smaller and only attract the electrolyte from a closer distance. Also, increasing the voltage would increase the thermal energy, resulting in thermal damages and larger overcutting [22]. Hence, to minimize the thermal damage, it is preferable to machine with lower sparking distance at lower voltage.

5.2. The effect of the tool size on the sparking distance

The sparking distances is observed for experiments done at 50 V and 1 M electrolyte concentration using five different tool sizes. The tool size is decreased from 1000 μm to 300 μm to find the sparking distance. A comparison of the sparking distance predicted by the model and the experimental observations for these different tool sizes is shown in Fig. 8. The error in predicting the average sparking distance is less than 3%. The maximum sparking distance (D_{max}) increases with the tool size. The tool size is known to be proportional to the surface tension and square to the electrostatics force and gravity force (Eq. (4)). The electrostatic and surface tension forces are found to be approximately 2 orders above the gravity force in the model. Therefore, the dominant effect of increasing the tool diameter is the increase of electrostatic force and surface tension, while the electrostatic force is at the square power. This increasing force will allow the electrolyte to be pulled up from a farther distance, as a result, increasing the maximum sparking distance.

5.3. The effect of the electrolyte concentration on the sparking distance

The sparking distances for the 0.5 M, 1 M and, 5 M electrolyte concentrations were tested.

Table 2 shows the average distance of sparking of 10 repetitions. The result shows that the electrolyte concentration has only a minor effect on the maximum sparking distance. The concentration of the electrolyte influences its conductivity. A higher concentration of free ions in the electrolyte can cause higher current flow and more gas bubble generation. However, since the tool was not immersed in the electrolyte, there is only a minor effect on the amount of current flow and gas bubble formation during the process with higher electrolyte concentration.

The electrolyte concentration affects the voltage range and critical voltage where the sparks appear. With the application of voltages, observations made through the high-speed camera revealed that the electrolyte level was invariably pulled up towards the tool face due to the electrostatic attraction and caused a reduction in the gap between the tool and the electrolyte. When the electrolyte touches the tool, ions are generated due to electrolysis. However, the wetted tool continues electrolysis and not sparking because the voltage has not passed the critical voltage (Fig. 9(a)). A possible reason is that the gap between the tool and the electrolyte lacks ions typically seen in the gas film during ECD [23]. Another important observation was that when the experiments were repeated with water instead of the NaOH solution, only the electrostatic attraction occurred, and there were no sparks in the entire range of 0–120 V, as seen in Fig. 9(b). Thus, it can be inferred that both the presence of ions in the electrolyte and the critical voltage are indispensable for sparking to occur in ECD (Fig. 9(c)).

6. Conclusions

A study on the sparking distance in the electrochemical discharging process was performed. The electrostatic force was found to affect the gas film formation and collapsing process. A mathematical model was developed to predict the sparking distance under the influence of electrostatic force and experimental verification of the theoretical model was carried out. It was found that the existence of layer of gas film alone does not guarantee a spark. The sparking will only happen if the applied voltage is higher than the critical voltage and the distance between the tool and electrolyte is smaller than the maximum sparking distance. The sparking distance is found to be the smallest at lower voltage and smaller tool sizes. Therefore, precision machining by ECD could be achieved by decreasing the applied voltage and tool size that reduces the sparking distance.

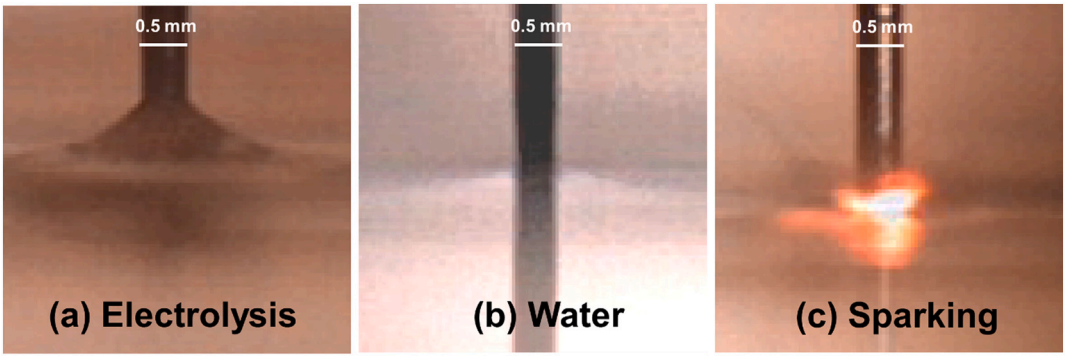

Fig. 9. The difference in NaOH (a) Only electrolysis occurs when the applied voltage is below the critical voltage (b) water pulled up to the tool, but no sparking is seen for 0–120 V. (c) sparks are noticed in NaOH for voltages above 40.

Declaration of competing interest

The authors declare that they have no known competing financial interests or personal relationships that could have appeared to influence the work reported in this paper.

Acknowledgments

This material is based upon work supported by the National Science Foundation [Grant No. CMMI-1833112]. Any opinions, findings, and conclusions or recommendations expressed in this material are those of the author(s) and do not necessarily reflect the views of the National Science Foundation.

References

[1] Rajurkar KP, Sundaram MM, Malshe AP. Review of electrochemical and electrodischarge machining. Procedia CIRP 2013;6:13–26. https://doi.org/10.1016/j.procir.2013.03.002 (2013/01/01).
[2] Hasan M, Zhao J, Jiang Z. A review of modern advancements in micro drilling techniques. Journal of Manufacturing Processes 2017;29:343–75. https://doi.org/10.1016/j.jmapro.2017.08.006 (2017/10/01).
[3] Sundaram M, Rajurkar KP. Electrical and electrochemical processes. In: Intelligent Energy Field Manufacturing and Interdisciplinary Process Innovations; 2010.
[4] Jui SK, Kamaraj AB, Sundaram MM. High aspect ratio micromachining of glass by electrochemical discharge machining (ECDM). Journal of Manufacturing Processes 2013;15(4):460–6. https://doi.org/10.1016/j.jmapro.2013.05.006 (2013/10/01).
[5] Singh T, Dvivedi A. On performance evaluation of textured tools during micro-channeling with ECDM. Journal of Manufacturing Processes 2018;32:699–713. https://doi.org/10.1016/j.jmapro.2018.03.033 (2018/04/01).
[6] Goud M, Sharma AK, Jawalkar C. A review on material removal mechanism in electrochemical discharge machining (ECDM) and possibilities to enhance the material removal rate. Precis Eng 2016;45:1–17. https://doi.org/10.1016/j.precisioneng.2016.01.007 (2016/07/01).
[7] Wüthrich R, Fascio V. Machining of non-conducting materials using electrochemical discharge phenomenon—an overview. Int J Mach Tool Manuf 2005;45(9):1095–108. https://doi.org/10.1016/j.ijmachtools.2004.11.011 (2005/07/01).
[8] Rajput V, Goud M, Suri NM. Review—electrochemical discharge machining: gas film electrochemical aspects, stability parameters, and research work. J Electrochem Soc 2021;168(1):013503. https://doi.org/10.1149/1945-7111/abd516 (2021/01/14).
[9] Kolhekar KR, Sundaram M. Study of gas film characterization and its effect in electrochemical discharge machining. Precis Eng 2018;53:203–11. https://doi.org/10.1016/j.precisioneng.2018.04.002 (in English).
[10] Han M-S, Min B-K, Lee SJ. Modeling gas film formation in electrochemical discharge machining processes using a side-insulated electrode. J Micromech Microeng 2008;18(4):045019. https://doi.org/10.1088/0960-1317/18/4/045019 (2008/03/11).
[11] Elhami S, Razfar MR. Numerical and experimental study of discharge mechanism in the electrochemical discharge machining process. Journal of Manufacturing Processes 2020;50:192–203. https://doi.org/10.1016/j.jmapro.2019.12.040 (2020/02/01).
[12] Jiang B, Lan S, Wilt K, Ni J. Modeling and experimental investigation of gas film in micro-electrochemical discharge machining process. Int J Mach Tool Manuf 2015;90:8–15. https://doi.org/10.1016/j.ijmachtools.2014.11.006 (2015/03/01).
[13] Kolhekar K, Sundaram M. A multiphase simulation study of electrochemical discharge machining of glass. The International Journal of Advanced Manufacturing Technology 2019;105(1):1597–608. https://doi.org/10.1007/s00170-019-04318-5 (2019/11/01).
[14] Basak I, Ghosh A. Mechanism of spark generation during electrochemical discharge machining: a theoretical model and experimental verification. J Mater Process Technol 1996;62(1):46–53. https://doi.org/10.1016/0924-0136(95)02202-3 (1996/11/01).
[15] Jain VK, Dixit PM, Pandey PM. On the analysis of the electrochemical spark machining process. Int J Mach Tool Manuf 1999;39(1):165–86. https://doi.org/10.1016/S0890-6955(98)00010-8 (1999/01/01).
[16] Wüthrich R, Fascio V, Bleuler H. A stochastic model for electrode effects. Electrochim Acta 2004;49(22):4005–10. https://doi.org/10.1016/j.electacta.2003.12.060 (2004/09/15).
[17] Appalanaidu B, Dvivedi A. On controlling of gas film shape in electrochemical discharge machining process for fabrication of elliptical holes. Materials and Manufacturing Processes 2021;36(5):558–71. https://doi.org/10.1080/10426914.2020.1854464 (2021/04/04).
[18] Nishiyama H, Nakamura M. Form and capacitance of parallel-plate capacitors. IEEE Transactions on Components, Packaging, and Manufacturing Technology: Part A 1994;17(3):477–84. https://doi.org/10.1109/95.311759.
[19] N. R. Council. International Critical Tables of Numerical Data, Physics, Chemistry and Technology. Washington, DC: The National Academies Press; 1930. p. 49 (in English).
[20] Don WG, Robert HP. Perry's Chemical Engineers' Handbook, Eighth Edition. 8th ed. New York: McGraw-Hill Education; 2008 (in en).
[21] Hector LG, Schultz HL. The dielectric constant of air at radiofrequencies. Physics 1936;7(4):133–6. https://doi.org/10.1063/1.1745374.
[22] Kamaraj AB, Jui SK, Cai Z, Sundaram MM. A mathematical model to predict overcut during electrochemical discharge machining. The International Journal of Advanced Manufacturing Technology 2015;81(1):685–91. https://doi.org/10.1007/s00170-015-7208-x (2015/10/01).
[23] Chen Y-J, Sundaram M. Experimental study on the mitigation of surface damages caused in electrochemical discharge machining of glass. Procedia CIRP 2020;95:731–6. https://doi.org/10.1016/j.procir.2020.02.257 (2020/01/01).